Harmonic Forcing Amplitude Effects in Globally Unstable Transonic Wing Flow

Panagiotis Belesiotis–Kataras* and Sebastian Timme†
School of Engineering, University of Liverpool, Liverpool L69 3GH, United Kingdom

Unsteady Reynolds-averaged Navier–Stokes simulations were carried out to investigate the aerodynamic response of a wing when a harmonic sinusoidal structural forcing using a synthetic torsion mode is imposed. Simulations were run for a number of excitation frequencies and amplitude factors. The flow conditions for the half wing-body model scaled to wind tunnel dimensions are a Mach number of 0.8 with a chord Reynolds number of 3.75×10^6 and angles of attack around onset of shock-buffet flow unsteadiness in the transonic regime. The finite-volume solver DLR–TAU was used for the simulations. The response signal of lift coefficient is analysed and discrete Fourier transformation allows the frequency content to be examined for both pre-onset and buffeting flows. For pre-buffet flow, time-marching non-linear simulation results are in agreement with those of the linearised frequency-domain method, for sufficiently low amplitudes, to give dynamic derivatives. More iterations are required for convergence as the excitation frequency is getting close to the buffet frequency range, pointing towards a weakly-damped dominant modal behaviour. For shock-buffet flow, low amplitude structural excitation appears to have negligible effect on the buffet dynamics while higher amplitude responses follow the harmonic forcing, with frequency content in the buffet range still present.

I. Introduction

The ever increasing needs of air transport require safer and more efficient aircraft that have a low environmental impact. The design optimization employed to achieve these goals goes hand in hand with pushing the flight envelope of the aircraft, especially by extending its capability to operate at high-speed edge-of-the-envelope conditions safely. To achieve that, a thorough understanding of the phenomena that are encountered in this transonic regime is needed. Shock buffet is an example of a transonic flow instability, mainly observed on supercritical wings in such high-speed edge-of-the-envelope conditions, emerging from the interaction of shock waves and separated boundary layers producing a self-excited, self-sustained mechanism. Separated flow due to these oscillations induces a drag penalty and the overall shock-buffet dynamics can excite the wing structure (called buffeting), resulting in e.g. an increase in fuel consumption and emissions, poorer aerodynamic performance, and a general degrading of the handling qualities of the aircraft. While the phenomenon of shock buffet was discovered over six decades ago [1], the physics that govern its mechanisms remain elusive. To date, shock buffet is mitigated by limiting the flight envelope of the aircraft, allowing a 30% margin from the cruise point to buffet onset in the design process [2]. Therefore, due to the need of optimization of future aircraft wings, the phenomenon of shock buffet has gained significant research interest.

While both numerical and experimental studies on two-dimensional aerofoils demonstrated that shock buffet has a characteristic shedding frequency with a weak dependence on geometry [3], discrepancies were observed regarding the order of magnitude of the frequency for its three-dimensional counterpart (i.e. Strouhal number range 0.06 to 0.08 for aerofoils and 0.2 to 0.7 for finite wings). These differences were later attributed to wing sweep, with three-dimensional effects becoming dominant for sweep angles of 20° and above. It is worth pointing out here that modern large aircraft have a typical sweep angle of about 30°. The shock-wave/boundary-layer interaction that takes places on a finite wing with an unavoidable flexible structure gives rise to aeroelastic phenomena. This interaction between the fluid and the elastic wing structure is expected as the order of magnitude of the shock-buffet shedding frequency range lies in the same range as higher frequency modes of transport aircraft that operate at transonic speeds [4]. Hence a multidisciplinary analysis that scrutinises the fluid-structure interaction dynamics is important.

Most numerical [5–10] and experimental [11–15] studies on the topic of transonic shock buffet over the years have focused on elucidating the governing physics of the phenomenon as well as predicting its onset. In an effort to classify the flow features, shock-buffet studies utilized rigid aerofoils and wings, excluding the effects of any interactions with the

*PhD Student, P.Belesiotis-Kataras@liverpool.ac.uk
†Senior Lecturer in Aerospace Engineering, Sebastian.Timme@liverpool.ac.uk. Member AIAA.

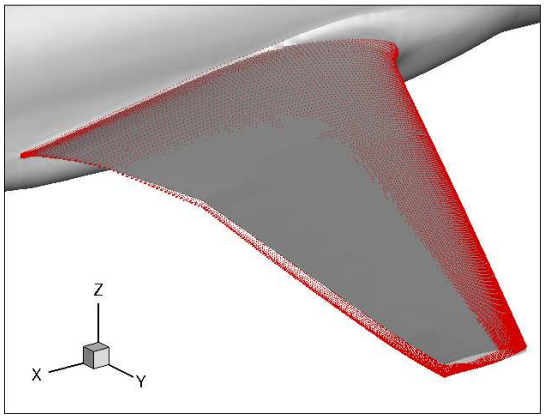

Fig. 1 Illustration of wing deformation due to synthetic torsion mode for an amplitude factor of $q_0 = 10$ for RBC12.

elastic wing structure. One of the first studies that looked further into fluid-structure interaction in unsteady periodic flows scrutinised the flow around an elastically suspended circular cylinder [16]. The lock-in behaviour observed, namely the synchronisation of the vortex shedding frequency to the natural vibration frequency of the structure (or the frequency that the structure is excited at) resulting in oscillations of increased amplitude, was attributed to resonance due to vortex induced vibration [17]. While additional studies on aerofoils speculated that a resonance mechanism is excited by shock buffet, the asymmetric nature of the lock-in boundaries [18], being shifted towards higher frequencies [19, 20], could not be fully explained by the resonance idea. More specifically, both single and two degree-of-freedom (pitch and pitch-and-heave) aerofoil systems did not demonstrate significant oscillations for lower forcing frequencies but increased amplitudes were observed for higher frequencies [19]. It is also important to mention that lock-in was observed when the excitation amplitude was above some threshold. In addition, experimental studies on flexible swept wings showed that at high-speed conditions, where a strong shock-wave/boundary-layer interaction is present, there was a strong fluid-structure coupling, with the frequency of the aeroelastic response following that of the oscillating flow field and not a structural eigenmode [21]. Reduced order models of two-dimensional aeroelastic systems showed that many characteristics such as coupling frequency can be predicted through a linear stability analysis. The same study also showed that the synchronisation of the aerodynamic and structural systems, leading to a limit-cycle oscillation, was related to an unstable coupled fluid mode [22]. This was scrutinised recently showing that the buffet onset is reduced by an elastic structure and the fluid-structure interaction can destabilise an originally stable fluid mode [23].

We investigate the dynamic response to harmonic forcing of an aircraft wing near shock-buffet onset conditions in the presence of the flow instability. The understanding of the fluid response to structural excitation will help guide a fully coupled aeroelastic study. Amplitude factor studies for pre-onset conditions using time-marching simulations will demonstrate the regime when non-linear effects become dominant. The test case is briefly introduced, with previous work summarised, in Sec. II, and the methods used are outlined in Sec. III. Results are presented in Sec. IV.

II. Large Aircraft Wing Test Case

The RBC12 model, shown in figure 1, is a half wing-body configuration scaled to wind tunnel dimensions. It has a quarter-chord sweep angle of 25°, a reference area of 0.296 m^2, an aerodynamic mean chord of 0.279 m, a semi-span of 1.104 m (with plinth included) and an aspect ratio of 7.78 [14]. This wing geometry has been studied extensively by the authors in the past. Specifically, Reynolds-averaged Navier–Stokes (RANS) simulations [7] as well as delayed detached-eddy simulations [10, 24] showed that, for the RBC12 model, the self-sustained shock wave oscillations occurred just above an onset angle of approximately $\alpha = 3.0°$. Global stability computations revealed a band of weakly damped eigenvalues approaching the imaginary axis towards the unstable half plane [8]. Extensive analysis of a transonic wind tunnel campaign [15, 25], which guided the numerical studies, has been presented, too.

The computational grid is composed of about 2.7×10^6 points using an unstructured mesh produced with the Solar mesh generator and following industry accepted guidelines (for mesh details see [8]). The focus is on a Mach number of 0.8 and the Reynolds number (based on the mean aerodynamic chord) is 3.75×10^6. Two angles of attack of $\alpha = 3.0°$ and 3.1° are considered herein. Far-field conditions are applied at a distance of 25 times the semi-span of the model and a symmetry boundary condition is applied along the centre plane. Fully turbulent flow is assumed.

III. Methodology

Governing Equations

The governing equations are the RANS equations along with the negative Spalart–Allmaras (S–A) one-equation turbulence model for closure. For a physical domain $\Omega \subset \mathbb{R}^3$ defined by a smooth boundary $\partial\Omega(t)$, the state vector containing the conservative variables is defined as,

$$\boldsymbol{w} = [\rho, \rho u, \rho v, \rho w, \rho E, \rho\check{\nu}]^T \tag{1}$$

with ρ as the density, (u, v, w) as the Cartesian velocity components, E as the energy and $\check{\nu}$ as the S–A primitive working variable. The governing equations can be written in semi-discrete form as

$$\frac{\mathrm{d}M\boldsymbol{w}}{\mathrm{d}t} = -\boldsymbol{R}(\boldsymbol{w}, \boldsymbol{x}, \dot{\boldsymbol{x}}) \tag{2}$$

where M is the matrix containing the discrete control volumes coming from the finite-volume method. The residual vector $\boldsymbol{R}$ is defined as

$$\boldsymbol{R}(\boldsymbol{w}, \boldsymbol{x}, \dot{\boldsymbol{x}}) = \int_{\partial\Omega(t)} \left(\mathbf{f}_c \cdot \mathbf{n} - \mathbf{f}_v \cdot \mathbf{n} - \boldsymbol{w}(\dot{\boldsymbol{x}} \cdot \mathbf{n})\right) \mathrm{d}\partial\Omega - \int_{\Omega(t)} \mathbf{Q}\, \mathrm{d}\Omega \tag{3}$$

where the vectors $\boldsymbol{x}$ and $\dot{\boldsymbol{x}}$ denote the time-dependent mesh-point coordinates and corresponding velocities, respectively. Vectors $\mathbf{f}_c$ and $\mathbf{f}_v$ are the convective and viscous flux vectors, respectively. The source terms of the turbulence model are given by $\mathbf{Q}$. The surface area is denoted as $\partial\Omega$ and $\mathbf{n}$ is the unit vector normal to $\partial\Omega$.

For the time-marching unsteady simulations, the dual time-stepping method with second-order backward differentiation formula is defined as

$$\boldsymbol{R}^* = \boldsymbol{R}(\boldsymbol{w}, \boldsymbol{x}, \dot{\boldsymbol{x}}) + \frac{3(M\boldsymbol{w})^{n+1} - 4(M\boldsymbol{w})^n + (M\boldsymbol{w})^{n-1}}{2\Delta t} = 0 \tag{4}$$

where Δt is the time-step. The discrete control volumes are time-dependent to observe the geometric conservation law.

For the linearised frequency-domain (LFD) simulations, the state vector $\boldsymbol{w}$ is decomposed into a steady base flow and a small time-dependent perturbation, i.e. $\boldsymbol{w}(t) \approx \bar{\boldsymbol{w}} + \varepsilon\tilde{\boldsymbol{w}}(t)$, where $\varepsilon \ll 1$. The perturbation is described as an oscillator $\tilde{\boldsymbol{w}} = \hat{\boldsymbol{w}}\, e^{i\omega^* t}$, where ω^* is the excitation frequency. A similar decomposition is applied to the time-dependent coordinates $\boldsymbol{x}$ and discrete control volumes M. Following substitution into equation (2), while neglecting all terms beyond first order in ε, we find after some rearranging,

$$\left[i\omega^* \bar{M} + \left.\frac{\partial \boldsymbol{R}}{\partial \boldsymbol{w}}\right|_{\bar{\boldsymbol{w}}, \bar{\boldsymbol{x}}, \dot{\bar{\boldsymbol{x}}}}\right] \hat{\boldsymbol{w}} = -\left[\left.\frac{\partial \boldsymbol{R}}{\partial \boldsymbol{x}}\right|_{\bar{\boldsymbol{w}}, \bar{\boldsymbol{x}}, \dot{\bar{\boldsymbol{x}}}} + i\omega^* \left(\left.\frac{\partial \boldsymbol{R}}{\partial \dot{\boldsymbol{x}}}\right|_{\bar{\boldsymbol{w}}, \bar{\boldsymbol{x}}, \dot{\bar{\boldsymbol{x}}}} + \bar{\boldsymbol{w}} \left.\frac{\partial M}{\partial \boldsymbol{x}}\right|_{\bar{\boldsymbol{x}}}\right)\right] \hat{\boldsymbol{x}} \tag{5}$$

where $\hat{\boldsymbol{w}}$ and $\hat{\boldsymbol{x}}$ denote the complex-valued amplitudes. In compact form, the linear system of equations can be written as

$$A\hat{\boldsymbol{w}} = \hat{\boldsymbol{b}} \tag{6}$$

Details of this derivation can be found in Thormann and Widhalm [26].

Synthetic Torsion Mode

The synthetic torsion mode, used for the structural excitation of the wing, is shown in figure 1. The mode resembles a typical wing torsional deformation but the mode itself is not based on a finite-element analysis of the actual wing structure. Specifically in this study, excitation follows a forced sinusoidal torsion deformation of the wing with the axis of rotation located approximately at the quarter-chord line. The deformation of the wing is zero at the root while increasing linearly towards the wing tip [8]. The maximum deflection is equal the amplitude factor q_0, i.e. for $q_0 = 1$ there will be a twist angle of 1° at the wing tip. The forced sinusoidal pitching motion is defined as

$$q(t) = q_0 \sin(\omega^* t) \tag{7}$$

with the reduced frequency

$$\omega^* = \frac{2\pi f l_{\mathrm{ref}}}{U_\infty} \tag{8}$$

where U_∞ and l_{ref} are the freestream velocity and the reference length, respectively.

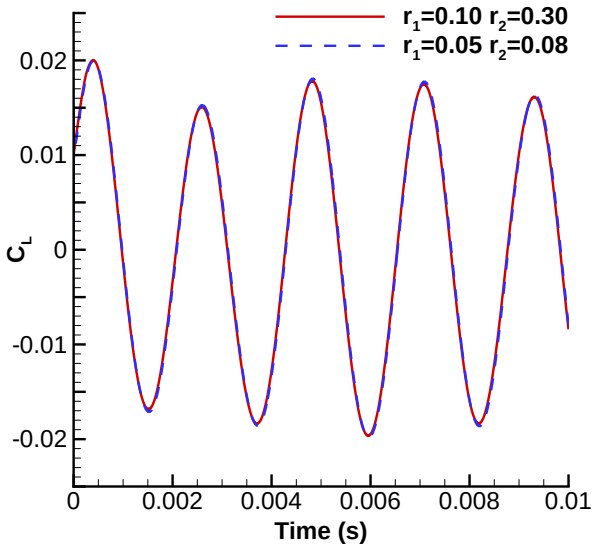

Fig. 2 Response of lift coefficient C_L over time for an excitation amplitude $q_0 = 1.0$ and frequency $\omega^* = 3.0$ from simulations using different mesh deformation settings for radii r_1 and r_2.

Simulation Tools

The unstructured finite-volume solver TAU, developed by the German Aerospace Center (DLR) and used both in industry and academia, was chosen for the simulations. Second-order spatial discretisation uses the standard central scheme with scalar artificial dissipation. The negative S–A one-equation model is discretised with a first-order upwind scheme. This was chosen as it has been shown in previous studies to capture shock buffet unsteadiness more accurately compared to a second-order scheme where buffet was not present along with lower amplitude lift and drag signals [10]. A compressibility correction has also been added in previous work [6, 27], but is not used herein. The Green–Gauss theorem is used for reconstructing the gradients of the flow variables. An implicit backward Euler solver converges the non-linear flow equations to steady state. Local time-stepping and geometric multigrid on three grid levels are employed to accelerate convergence. All steady solutions at $\alpha = 3.0°$ converged by at least ten orders of magnitude.

For unsteady time-marching simulations, FS Forced Motion from the FlowSimulator environment for multi-disciplinary simulations is used. This software enables computational fluid dynamics enhanced multidisciplinary simulations on massively parallel computing systems while providing a plug-in environment where different computational fluid dynamics tools and developer scripts can be utilised [28]. Dual time-stepping with second-order backward differentiation formula is employed, as given in equation (4). The aerodynamic system is then evaluated for each time step by iterating the pseudo residual $\boldsymbol{R}^*$ to a steady state at each time step. The physical time step follows from the excitation frequency and the chosen number of steps per cycle, as outlined below. Integrated aerodynamic loads, such as lift coefficient and generalised aerodynamic force projecting the surface flow solution onto the structural mode, are computed once the flow equations have converged at the end of each time step. For the unsteady RANS simulations, together with the convergence criterion on the norm of the density residual (10^{-3}), a Cauchy criterion is applied for the drag coefficient with error tolerance 10^{-9} with a minimum of 150 inner iterations per real time step.

For the solution of equation (6) for the RANS LFD simulations, a block incomplete lower-upper factorisation preconditions the chosen Krylov sparse iterative linear solver; specifically a generalized conjugate residual solver with deflated restarting was introduced in [29]. The required Jacobian matrix has been derived analytically in the code with details given in [26]. The linearised flow solver has been scrutinised previously both for an aerofoil and a wing in such edge-of-the-envelope flow conditions [8, 30–32]. Mesh deformation routine to account for the moving wing in computing the right-hand side forcing term $\hat{\boldsymbol{b}}$ in equation (6) uses a radial-basis-function (RBF) method [33].

For the non-linear time-marching simulations, different mesh deformation settings were used to allow the simulation of larger excitations. RBF is used to ensure smooth deformations even for the small wing deflections close to the fuselage in comparison to the overall larger deflection towards the wing tip. RBF requires the definition, amongst other

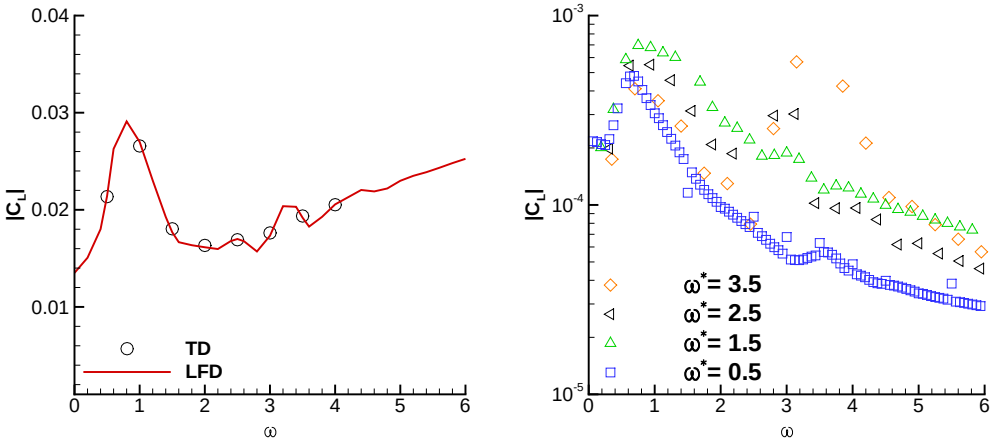

(a) Peaks at fundamental frequencies

(b) Lower amplitude response

Fig. 3 Magnitude of unsteady lift coefficient C_L from Fourier analysis of time-marching simulations at pre-onset conditions at different excitation frequencies for an amplitude factor $q_0 = 0.001$. The solid line represents unsteady lift results previously computed in [8] using RANS LFD simulations. The amplitude peaks at the respective fundamental frequencies for different excitation frequencies are shown in (a) while (b) shows a closer view of the additional lower amplitude frequency content.

parameters, of weighting radii. In the area defined by the full weight radius r_1, full deformation is applied, represented by a weighting of 1. The zero weight radius r_2 denotes a larger distance containing r_1. Within this radius, along the distance $r_2 - r_1$, the deformation weighting is linearly blended to the flow field from 1 to 0. The effect of the RBF settings, specifically different weighting radii, on the lift coefficient response is negligible, as shown in figure 2.

IV. Results

Simulations were carried out for two angles of attack, specifically, pre-onset condition at $\alpha = 3.0°$ and post onset at $\alpha = 3.1°$. For structural forcing with an amplitude factor $q_0 < 10^{-1}$, simulations were run with 1024 time steps per cycle of oscillation, whereas for $q_0 \geq 0.1$, 2048 steps were used. All simulations continued for eight to nine cycles. For pre-onset conditions, simulations were conducted at four reduced frequencies $\omega^* = 0.5$, 1.5, 2.5 and 3.5 excited at different amplitude factors $q_0 = 10^{-5}, 10^{-3}$ and 10^{-1}. For $q_0 = 10^{-3}$, simulations at four additional frequencies $\omega^* = 1.0$, 2.0, 3.0 and 4.0 were carried out. At post-onset conditions, the frequencies of interest were chosen according to the frequency content of a static shock-buffet simulation. In this, the governing flow equations were marched in time without any forcing, and therefore, by analysing the resulting lift coefficient, the frequency content of the oscillating flow field, which in this case is the shock buffet range, can be recovered. This was found to centre around $\omega^* = 3.0$ (corresponding to a Strouhal number of $St = 0.477$) with the highest amplitude response being at this frequency. The three excitation frequencies were chosen around this buffet frequency peak with increments of 0.5, giving $\omega^* = 2.5$, 3.0 and 3.5. Lastly, for these conditions, the excitation amplitude factor ranges from $q_0 = 10^{-3}$ to 1.0 in increasing orders of magnitude with an additional higher amplitude simulation at $q_0 = 5.0$.

Validation of Results

Unsteady time-marching results for different excitation frequencies for an amplitude factor of $q_0 = 0.001$ at pre-onset conditions computed using Flow Simulator were compared with previous LFD results [8] produced with DLR–TAU for validation. Figure 3(a) shows the magnitude of the lift coefficient, $|C_L|$, at the respective fundamental frequencies of the excitation obtained from a discrete Fourier transform on the lift signal for a number of excitation frequencies. Comparison of the results obtained from time-marching simulations with the LFD results shows that the two methods are in excellent agreement. The dynamic derivative calculated using the LFD method predicts a low frequency resonant peak between $\omega^* = 0.4$ and 1.6 along with higher frequency wiggles between $\omega^* = 2.6$ and 3.8. This behaviour is also found for the lower amplitude content from the time-dependent simulations at four frequencies,

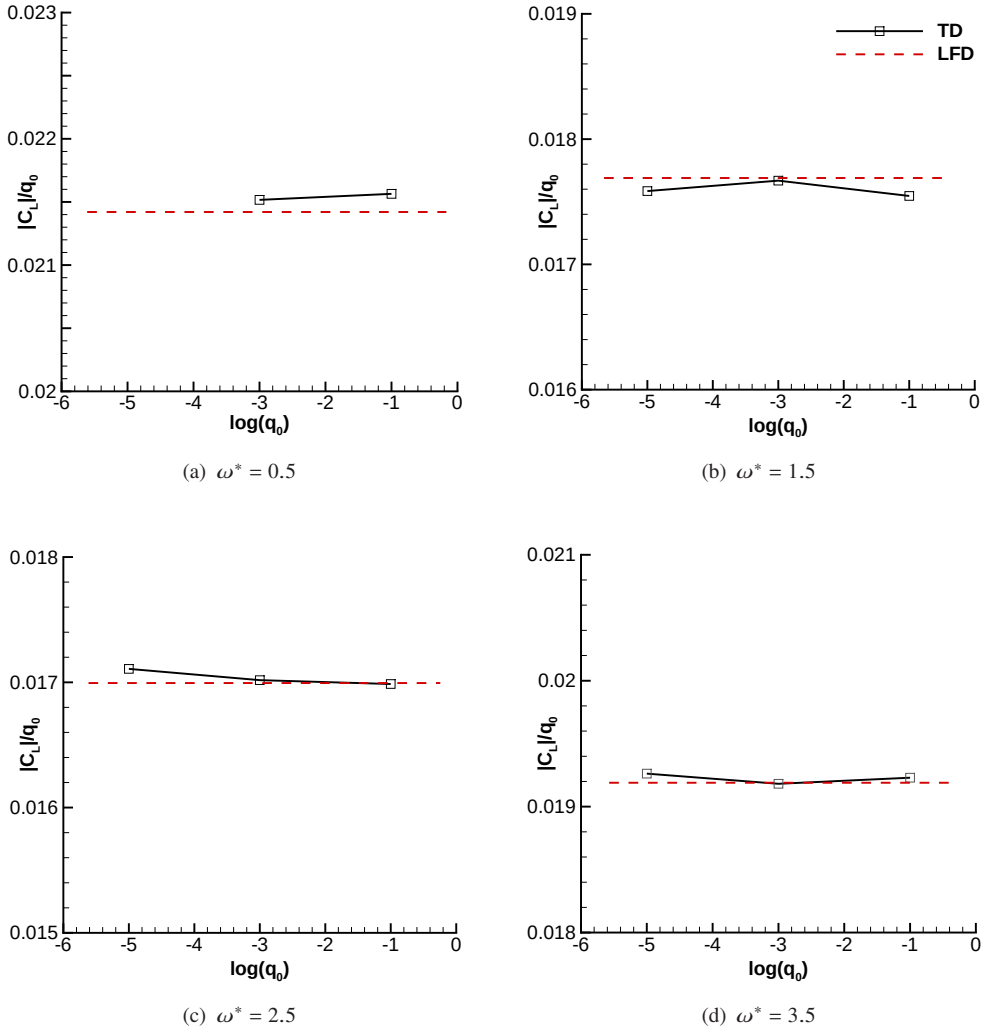

(a) $\omega^* = 0.5$ (b) $\omega^* = 1.5$

(c) $\omega^* = 2.5$ (d) $\omega^* = 3.5$

Fig. 4 Comparison of lift coefficient magnitude from LFD results with time-marching simulations, normalised by excitation amplitude for amplitude factors $q_0 = 10^{-5}, 10^{-3}$ and 10^{-1} and different excitation frequencies ω^*.

shown in figure 3(b). There it can be seen that at pre-onset a lower frequency bump in the same range as the LFD resonant peak is present and consistent for all forcing frequencies, and forcing frequencies close to the buffet range excite buffet dynamics, something that agrees with the behaviour observed in previous studies [8, 34].

Pre-onset Conditions

The simulations in pre-onset conditions examine the effect of the excitation amplitude in a globally stable flow. Figure 4 shows the lift coefficient magnitude normalised by excitation amplitude (i.e. dynamic derivative) as a function of amplitude factor, specifically $q_0 = 10^{-5}, 10^{-3}$ and 10^{-1}, at four chosen frequencies. The magnitudes from the time-marching simulations for the range of different q_0 agree nicely with the LFD results. Figure 5 shows the corresponding sum of the higher harmonics of the fundamental excitation frequency over time periods. As the frequency increases towards the typical shock-buffet range, higher harmonics of similar magnitude are excited for all excitation amplitudes. It is here worth pointing out that more iterations are required for the response to settle as we get closer to the shock-buffet range. Due to the computational cost of the simulations, we aimed for a compromise between the highest accuracy and increasing computational cost. The chosen simulation setup is such a robust compromise.

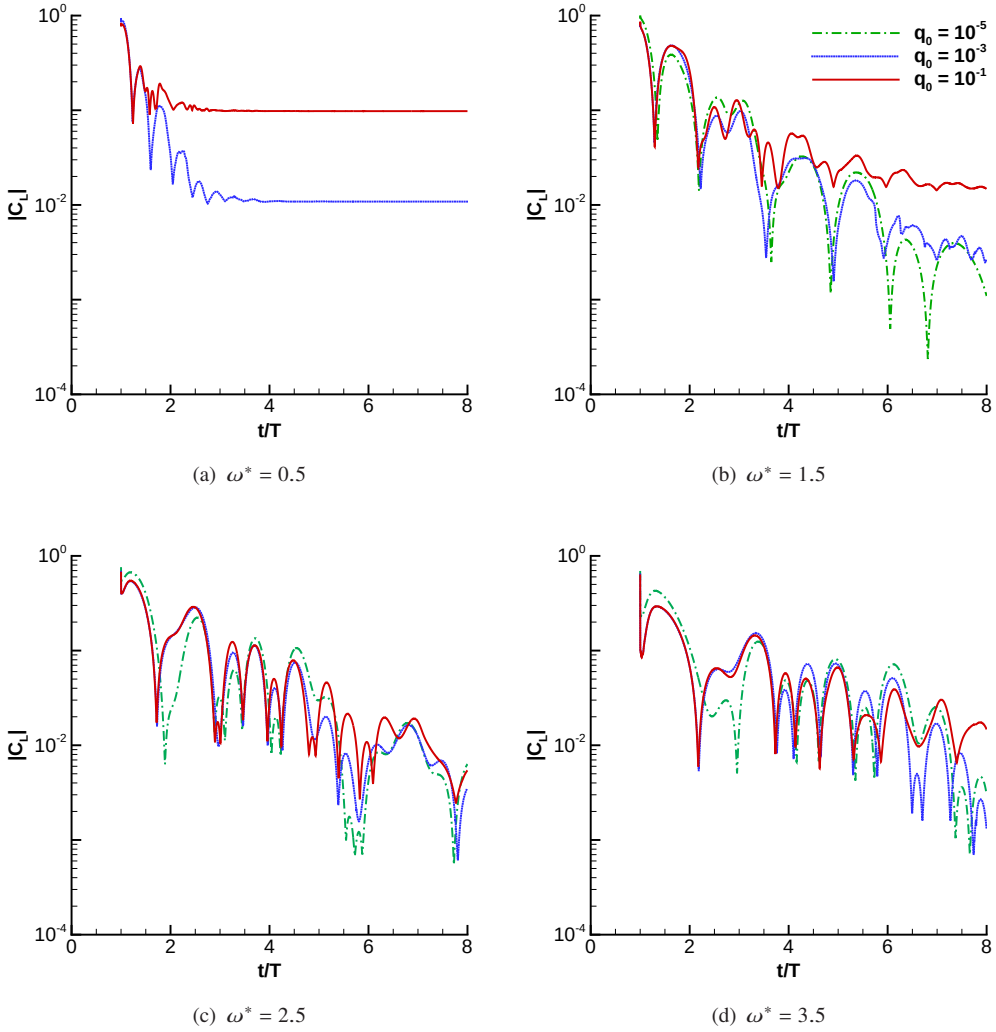

(a) $\omega^* = 0.5$ (b) $\omega^* = 1.5$

(c) $\omega^* = 2.5$ (d) $\omega^* = 3.5$

Fig. 5 Comparison of the sum of higher harmonics of the excitation frequency over computational cycles.

Buffeting Flow Conditions

The unsteady response to harmonic forcing, in globally unstable flow exhibiting shock buffet, is discussed next. Figure 6 shows the response of the lift coefficient following a harmonic forcing with increasing amplitude factor q_0. The left column presents the time histories of the raw data, whereas the right column gives processed results, with the lift response scaled by q_0 and the time normalised by the period of oscillation. For $q_0 = 0.001$ the response follows that of the static shock-buffet simulation which in this case is the lift variation due to the shock-buffet unsteadiness, shown in figure 6(a). With increasing amplitude factor, the lift response starts desynchronising from the buffet dynamics and follows the structural excitation instead. Initial synchronisation can be seen in figure 6(b) while distinctly different responses compared to the static simulation are evident in figure 6(c). For the largest amplitude factors, $q_0 = 1.0$ and 5.0, the response is fully aligned with the forcing, as can be clearly seen in the scaled results.

Discrete Fourier analysis of the unsteady lift coefficient returns the frequency content for each combination of forcing amplitude factor and frequency. In the left column of figure 7, the frequency content of the lift coefficient (specifically its magnitude) for fixed amplitudes in increasing order is shown. It can be seen that for the two lower amplitude factors, $q_0 = 0.001$ and 0.01, the wing motion hardly modifies the buffet dynamics. There is strong similarity with the static simulation results. As the amplitude factor is increased to 0.1, peaks at the respective excitation frequencies are present. In addition, unsteady content is excited at higher amplitudes compared with the static signal. As we further increase to an amplitude factor of $q_0 = 1.0$, the peaks at the respective excitation frequencies become more distinct and larger in

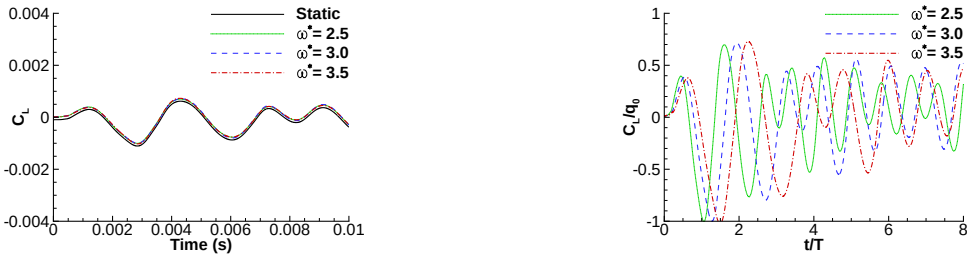

(a) $q_0 = 0.001$

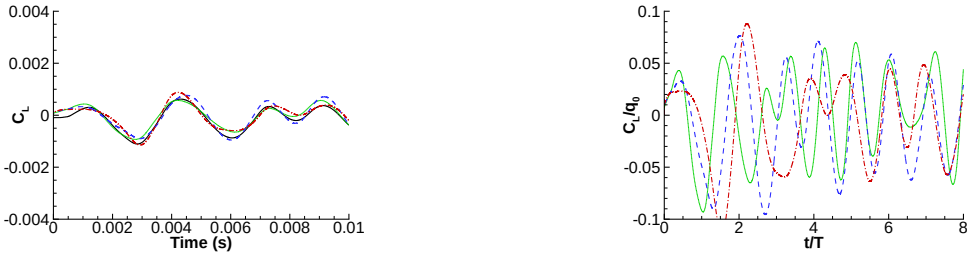

(b) $q_0 = 0.01$

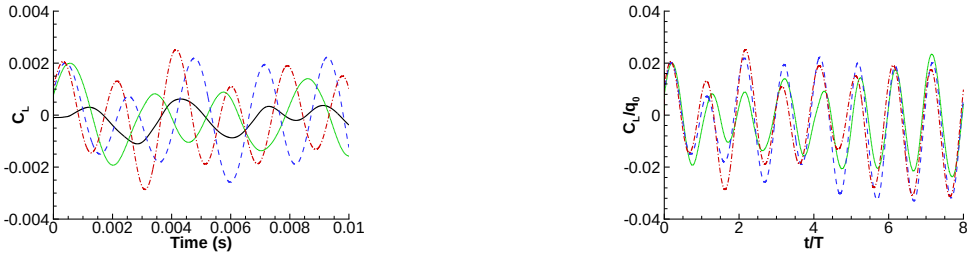

(c) $q_0 = 0.1$

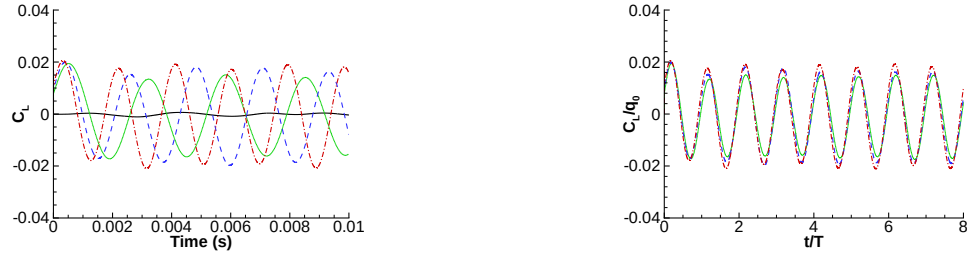

(d) $q_0 = 1.0$

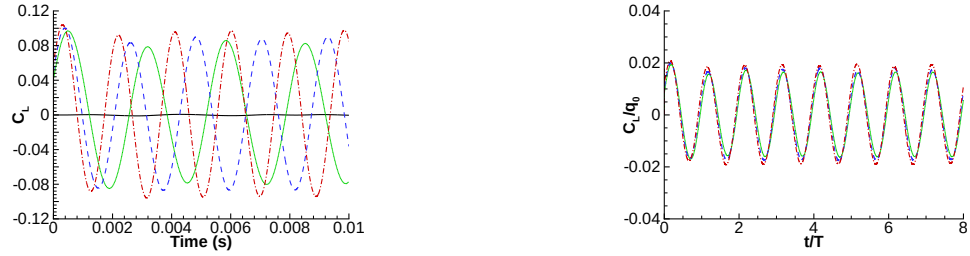

(e) $q_0 = 5.0$

Fig. 6 Response of lift coefficient C_L to harmonic excitation over time (left column) and corresponding lift coefficient normalised by excitation amplitude over periods (right column) at different excitation frequencies at $\alpha = 3.1°$.

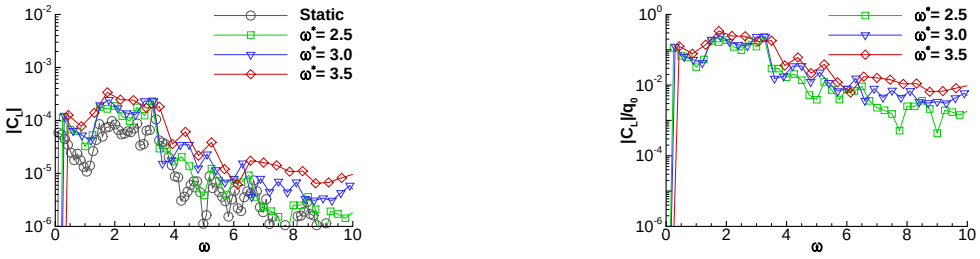

(a) $q_0 = 0.001$

(b) $q_0 = 0.01$

(c) $q_0 = 0.1$

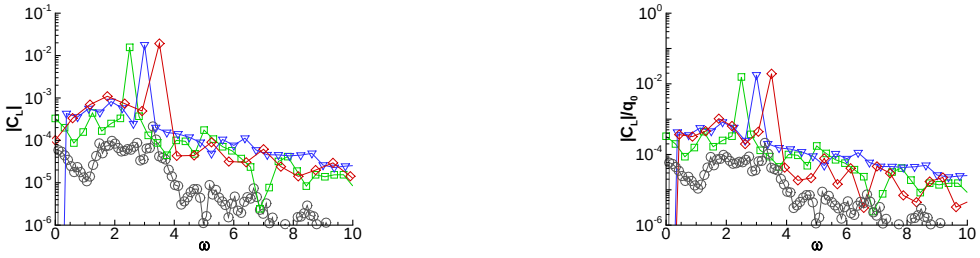

(d) $q_0 = 1.0$

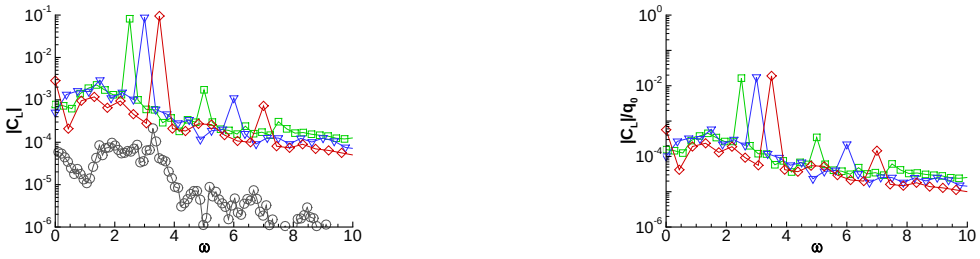

(e) $q_0 = 5.0$

Fig. 7 Frequency response of lift coefficient C_L to harmonic excitation (left column) and corresponding frequency response of lift coefficient normalised by excitation amplitude (right column) at $\alpha = 3.1°$

magnitude whereas the amplitude of the unsteady content that is excited has the same magnitude as for $q_0 = 0.1$. The same behaviour follows for the largest amplitude factor of 5.0, except that additional peaks at the higher harmonics of the excitation frequencies are present compared to $q_0 = 1.0$. In addition the amplitude of the buffet content that is excited increases in order of magnitude. Fourier analysis of the scaled results allows similar conclusions. The peaks at the excitation frequencies approximate the dynamic derivatives for $q_0 \geq 0.1$, while the overall level of unsteadiness, relative to the excitation, at the non-excited frequencies seems to be reduced with increasing forcing amplitude.

Discussion

Unsteady time-marching simulations due to harmonic structural forcing for pre and post buffet onset conditions were carried out to investigate the flow response at the respective conditions. A comparison with previous LFD results demonstrates the weakly damped modal behaviour of shock buffet close to onset. This can be seen in figure 3(b) as excitation frequencies close to the buffet frequency range excite high frequency buffet content related to an absolute instability along with low frequency (possibly) pseudo-resonance content. This agrees with observations from previous stability study [8] that shows a group of weakly damped eigenvalue approaching the unstable half-plane as the angle of attack is increased. The effects of this behaviour are shown in figure 5 where more iterations are required for the response to settle as the forcing frequency approaches the buffet range and a broader frequency content is excited even for small amplitude factors. Results for forcing frequencies at different amplitude factors at the same conditions in figure 4 agree with the dynamic-derivative value calculated using the LFD method for all amplitudes, as no non-linearities are excited for the largest amplitude factor.

The response of globally unstable flow to harmonic forcing gives a different behaviour to its pre-onset counterpart. In this regime, small amplitude excitations ($q_0 < 0.001$) do not appear to have an effect as the dynamics follows that of the static simulation, namely the shock buffet response. With increasing forcing amplitude ($q_0 > 0.01$), the flow response starts following the harmonic excitation. Scrutinising the frequency content also shows that low frequency content is excited even for the largest amplitude factors. This suggests a different behaviour to what other studies have demonstrated in two-dimensional analyses. More specifically, a complete synchronisation, or 'lock-in', of the structural and aerodynamic systems is not observed herein with the chosen simulation parameters and assumptions.

V. Conclusions

Shock-buffet dynamics, and its interaction with wing vibration, has been analysed herein. Specifically, the aerodynamic response to harmonic structural excitation via a synthetic torsional mode at pre-onset and unsteady flow conditions for a civil aircraft wing has been scrutinised. Results are presented for a range of forcing amplitude factors and frequencies. For a pre-buffet flow, results produced from time-domain simulations at different excitation frequencies are compared with linearised frequency-domain results from previous studies. Overall good agreement is found in predicting the dynamics derivatives. The weakly damped modal behaviour of shock buffet close to onset is translated into increased iteration counts for the response to converge to the periodic state. For the shock-buffet flow conditions, the wing is excited around the typical buffet frequencies. A comparison of the various lift responses showed that for lower amplitude forcing, shock buffet dominates the dynamics, whereas the aerodynamic response starts following the excitation with increasing forcing amplitude. By analysing the frequency content of the aforementioned responses it is revealed that lower frequency content is present even for the larger amplitude factors where the lift coefficient response tracks that of the structural excitation. Lastly, while this study aids the understanding of the effects of structural forcing on quasi-rigid wings in globally unstable flow, a full aeroelastic analysis that will explore the impact of shock buffet on the coupled dynamics is desirable. Insight gained herein will guide such future simulation.

Acknowledgements

The authors wish to acknowledge Airbus Group for sponsoring the PhD studentship. We also wish to thank Aircraft Research Association for making the RBC12 model available for this study.

References

[1] Hilton, W. F., and Fowler, R., *Photographs of shock wave movement*, HM Stationery Office, 1952.

[2] EASA, "Certification Specifications for Large Aeroplanes," , 2009.

[3] Garnier, E., and Deck, S., "Large-eddy simulation of transonic buffet over a supercritical airfoil," *Turbulence and interactions*, Springer, 2010, pp. 135–141.

[4] Banerjee, J., Liu, X., and Kassem, H., "Aeroelastic Stability Analysis of High Aspect Ratio Aircraft Wings," *Journal of Applied Nonlinear Dynamics*, Vol. 3, 2014, pp. 413–422.

[5] Iovnovich, M., and Raveh, D. E., "Numerical study of shock buffet on three-dimensional wings," *AIAA Journal*, Vol. 53, No. 2, 2015, pp. 449–463.

[6] Crouch, J., Garbaruk, A., Magidov, D., and Travin, A., "Origin of transonic buffet on aerofoils," *Journal of Fluid Mechanics*, Vol. 628, 2009, pp. 357–369.

[7] Sartor, F., and Timme, S., "Reynolds-averaged Navier-Stokes simulations of shock buffet on half wing-body configuration," *53rd AIAA Aerospace Sciences Meeting*, 2015. AIAA 2016-1939.

[8] Timme, S., and Thormann, R., "Towards three-dimensional global stability analysis of transonic shock buffet," *AIAA Atmospheric Flight Mechanics Conference*, 2016, p. 3848.

[9] Brunet, V., and Deck, S., "Zonal-detached eddy simulation of transonic buffet on a civil aircraft type configuration," *Advances in Hybrid RANS-LES Modelling*, Springer, 2008, pp. 182–191.

[10] Sartor, F., and Timme, S., "Delayed detached–eddy simulation of shock buffet on half wing–body configuration," *AIAA Journal*, Vol. 55, No. 4, 2016, pp. 1230–1240.

[11] Roos, F., "Surface pressure and wake flow fluctuations in a supercritical airfoil flowfield," *13th Aerospace Sciences Meeting*, 1975, p. 66.

[12] McDevitt, J. B., and Okuno, A. F., "Static and dynamic pressure measurements on a NACA 0012 airfoil in the Ames high Reynolds number facility," 1985.

[13] Lee, B., "Transonic buffet on a supercritical aerofoil," *The Aeronautical Journal*, Vol. 94, No. 935, 1990, pp. 143–152.

[14] Lawson, S., Greenwell, D., and Quinn, M. K., "Characterisation of buffet on a civil aircraft wing," *54th AIAA Aerospace Sciences Meeting*, 2016. AIAA 2016-1309.

[15] Masini, L., Timme, S., Ciarella, A., and Peace, A., "Influence of vane vortex generators on transonic wing buffet: further analysis of the BUCOLIC experimental dataset," *Proc. of the 52nd 3AF International Conf. on Applied Aerodynamics*, 2017.

[16] Blevins, R. D., "Flow-induced vibration," *New York, Van Nostrand Reinhold Co., 1977. 377 p.*, 1977.

[17] Govardhan, R., and Williamson, C., "Resonance forever: existence of a critical mass and an infinite regime of resonance in vortex-induced vibration," *Journal of Fluid Mechanics*, Vol. 473, 2002, pp. 147–166.

[18] Raveh, D., and Dowell, E., "Frequency lock-in phenomenon for oscillating airfoils in buffeting flows," *Journal of Fluids and Structures*, Vol. 27, No. 1, 2011, pp. 89–104.

[19] Raveh, D. E., and Dowell, E. H., "Aeroelastic responses of elastically suspended airfoil systems in transonic buffeting flows," *AIAA Journal*, Vol. 52, No. 5, 2014, pp. 926–934.

[20] Quan, J., Zhang, W., Gao, C., and Ye, Z., "Characteristic analysis of lock-in for an elastically suspended airfoil in transonic buffet flow," *Chinese Journal of Aeronautics*, Vol. 29, No. 1, 2016, pp. 129–143.

[21] Steimle, P. C., Karhoff, D.-C., and Schröder, W., "Unsteady transonic flow over a transport-type swept wing," *AIAA journal*, Vol. 50, No. 2, 2012, pp. 399–415.

[22] Gao, C., Zhang, W., Li, X., Liu, Y., Quan, J., Ye, Z., and Jiang, Y., "Mechanism of frequency lock-in in transonic buffeting flow," *Journal of Fluid Mechanics*, Vol. 818, 2017, pp. 528–561.

[23] Nitzsche, J., Ringel, L. M., Kaiser, C., and Hennings, H., "Fluid-mode flutter in plane transonic flows," *International Forum on Aeroelasticity and Structural Dynamic, IFASD2019*, 2019.

[24] Masini, L., Timme, S., and Peace, A. J., "Reynolds Number Effects on Wing Shock Buffet Unsteadiness," *AIAA Aviation 2019 Forum*, 2019. doi:10.2514/6.2019-2820, AIAA 2019-2820.

[25] Masini, L., Timme, S., and Peace, A. J., "Analysis of a civil aircraft wing transonic shock buffet experiment," *Journal of Fluid Mechanics*, 2019. doi:10.1017/jfm.2019.906.

[26] Thormann, R., and Widhalm, M., "Linear-frequency-domain predictions of dynamic-response data for viscous transonic flows," *AIAA Journal*, Vol. 51, No. 11, 2013, pp. 2540–2557.

[27] Crouch, J. D., Garbaruk, A., and Strelets, M., "Global instability in the onset of transonic-wing buffet," *Journal of Fluid Mechanics*, Vol. 881, 2019, pp. 3–22.

[28] Meinel, M., and Einarsson, G. O., "The FlowSimulator framework for massively parallel CFD applications," *PARA 2010 conference*, 2010, pp. 6–9.

[29] Xu, S., Timme, S., and Badcock, K. J., "Enabling off-design linearised aerodynamics analysis using Krylov subspace recycling technique," *Computers & Fluids*, Vol. 140, 2016, pp. 385–396.

[30] Thormann, R., and Timme, S., "Efficient aerodynamic derivative calculation in three-dimensional transonic flow," *The Aeronautical Journal*, Vol. 121, No. 1244, 2017, pp. 1464–1478.

[31] Timme, S., "Global Instability of Wing Shock Buffet," *arXiv eprint arXiv:1806.07299*, 2018.

[32] Timme, S., "Global Shock Buffet Instability on NASA Common Research Model," *AIAA Scitech 2019 Forum*, AIAA Paper 2019–0037, San Diego, California, 2019. doi:10.2514/6.2019-0037.

[33] Michler, A. K., "Aircraft control surface deflection using RBF-based mesh deformation," *International Journal for Numerical Methods in Engineering*, Vol. 88, No. 10, 2011, pp. 986–1007.

[34] Belesiotis-Kataras, P., and Timme, S., "Numerical Study of Incipient Transonic Shock Buffet on Large Civil Aircraft Wings," *Royal Aeronautical Society Applied Aerodynamics Conference*, 2018.